Decentralized Impulse Control for Multiagent Space Systems

Xun Liu
Department of Mechanical Engineering
Villanova University
Villanova, PA 19085-1681
(610) 519-4980
FAX: (610) 519-7312
xliu8@villanova.edu

Bo Wang
Department of Mechanical Engineering
The City College of New York
New York, NY 10031
(212) 650-5204
bwang1@ccny.cuny.edu

Hashem Ashrafiuon
Department of Mechanical Engineering
Villanova University
Villanova, PA 19085-1681
(610) 519-7791
FAX: (610) 519-7312
hashem.ashrafiuon@villanova.edu

Sergey G. Nersesov
Department of Mechanical Engineering
Villanova University
Villanova, PA 19085-1681
(610) 519-8977
FAX: (610) 519-7312
sergey.nersesov@villanova.edu

Abstract— **For nonlinear systems that admit continuous-time stabilizing controllers, we propose a Lyapunov-based technique to map this continuous-time control input into a sequence of discrete impulses while guaranteeing the desired performance of the closed-loop system. Specifically, a numerical algorithm, running in real-time, determines the instants of control impulse injections into the system based on comparison of a Lyapunov function value predicated on continuous-time control and on impulse control. No control input is applied to the system throughout the operation except for these occasional impulsive control injections. The main advantage of the proposed technique is two-fold: first, it allows to significantly reduce control effort while still achieving the desired control objective and secondly, our method takes into account the control saturation limits as part of the underlying design. We apply this technique to design decentralized cooperative control for the formation flying of multiple satellites and spacecraft distributed along the orbit. These vehicles typically use discrete burns to reduce fuel consumption, and hence, the proposed technique is well-suited for such application. We demonstrate its efficacy through numerical simulations.**

1. INTRODUCTION

Lyapunov theory serves as a fundamental tool for the development of continuous-time control strategies for nonlinear systems [1, 2]. However, continuous-time control may be inefficient or infeasible in certain applications. For instance, satellites and spacecraft often rely on impulsive discrete controllers for tasks such as station-keeping, orbital transfers, or collision avoidance maneuvers. In these scenarios, impulsive thrusters provide control forces and moments for brief durations, while most of the time, the control input remains zero to conserve fuel. Another example where continuous-time control is impractical involves rockets, missiles, and vehicles guided by single-use thrusters [3, 4]. These thrusters function as miniature explosive devices attached to the vehicle, using the reaction force from the explosion to guide its trajectory. Similar to satellite applications, the control input from the reaction force is applied over a short period of time, with no control effort during the remaining time.

One method for converting continuous-time inputs into a sequence of impulsive inputs is through sampled-data control [5, 6]. In this approach, a discrete-time control input is designed for a discretized model of the continuous-time system and implemented on the continuous-time model using a zero-order hold. While this method has been effective, it presents two main challenges. First, it is not yet definitively proven that the discrete-time control input, combined with zero-order hold, asymptotically stabilizes the continuous-time system, a critical aspect often overlooked in practice. Second, this approach necessitates the piecewise continuous implementation of the control input, which may not be feasible in applications with limited control resources, such as missiles or rockets guided by single-use thrusters.

To address the latter issue, the concept of hands-off control was introduced [7–9], which involves applying a constant control input for a finite time period while maintaining zero control for the majority of the time. The idea is that the duration of zero control is significantly longer than the periods of active control. A related concept, maximum hands-off control [10, 11], aims to maximize the sparsity of control inputs, prolonging the intervals during which no control is applied. This idea is tied to the earlier notion of minimum attention control [12], a concept specialized for linear systems [13], which argues that the simplest form of control is constant control. Other approaches, such as event-triggered control [14] and self-triggered control [15], focus on designing feedback controllers that determine the control input value and the precise moment when it should be applied.

In this paper, we propose a new technique, based on Lyapunov theory, to map continuous-time control inputs into a sequence of impulses while ensuring the desired closed-loop performance. A real-time numerical algorithm determines the timing of control impulse injections by comparing the value of a Lyapunov function under continuous-time control with that under the impulse control. The control objective is to ensure that the Lyapunov function value under impulse control remains lower than that of the continuous-time control. Since the continuous-time control converges to zero over time, the impulse control guarantees that the Lyapunov function value is driven to zero, thereby achieving the desired system performance. This approach reduces the control effort compared to continuous-time controllers by applying control as discrete pulses of short duration. Additionally, the method incorporates actuator saturation limits, making it suitable for

2025 IEEE Aerospace Conference | 979-8-3503-5597-0/25/$31.00 ©2025 IEEE | DOI: 10.1109/AERO63441.2025.11068503

979-8-3503-5597-0/25/$31.00 ©2025 IEEE

Authorized licensed use limited to: City College of New York. Downloaded on January 26,2026 at 02:38:13 UTC from IEEE Xplore. Restrictions apply.

real-world systems with practical control constraints.

The satellite constellation composed of small satellites has received considerable attention over the past decade. Compared to bulky individual satellites such constellations offer advantages in terms of lower launch costs and increased system flexibility and reliability. Consequently, numerous formation-flying missions have been developed and successfully conducted. In this paper, we implement the proposed Lyapunov-based thruster management methodology in the problem of decentralized satellite formation flying control. Numerical simulations are performed to demonstrate the effectiveness of the proposed approach. By comparing the results of the impulsive controller with those of the continuous-time controller, it is evident that the impulsive controller shows significant potential for reducing energy consumption. Furthermore, the inherent feature of the proposed approach takes into account the control saturation limits which is another key advantage, compared to traditional continuous-time control based on Lyapunov theory.

The structure of the remaining paper is as follows. Section 2 presents the methodology for transforming a continuous-time controller into an impulse sequence. Section 3 provides a general introduction to the modeling and equations of motion, along with the approaches used in developing the continuous-time controller. Simulations of decentralized satellite formation flying and comparative results are discussed in Section 4, and conclusions are drawn in Section 5.

2. TRANSFORMING CONTINUOUS-TIME CONTROL INTO AN IMPULSE SEQUENCE

In this section, we present a technique for transforming a stabilizing continuous-time control input into a sequence of discrete impulses, i.e., pulse inputs of short time duration, to stabilize a nonlinear system. This approach is particularly relevant, and often essential, in scenarios such as the satellite formation flying control. Generally, consider a nonlinear dynamical system of the form

$$\dot{x}(t) = f(t, x(t), u(t)), \quad x(0) = x_0, \quad t \geq t_0, \tag{1}$$

where $x(\cdot) \in \mathbb{R}^n$ represents the state and $u(\cdot) \in \mathbb{R}^m$ denotes the control input. Assume that there exists a continuous-time feedback control law $u(t) = \phi(x(t))$ such that the origin of the closed-loop system

$$\dot{x}(t) = f(t, x(t), \phi(x(t))), \quad x(0) = x_0, \quad t \geq t_0, \tag{2}$$

is asymptotically stable within a domain $\mathcal{D} \subseteq \mathbb{R}^n$. According to the converse Lyapunov theorem (see Theorem 4.8 in [2]), there exists a positive definite function $V_c : \mathcal{D} \to \mathbb{R}$ and a class $\mathcal{K}$ function $\gamma(\cdot)$ such that

$$\dot{V}_c(x) = V_c'(x) f(t, x, \phi(x)) \leq -\gamma(\|x\|),\ x \in \mathcal{D},\ t \geq t_0. \tag{3}$$

In practical applications, to establish the stability of a control input $u(t) = \phi(x(t))$, it is often necessary to identify a Lyapunov function $V_c : \mathcal{D} \to \mathbb{R}$ such that the stability condition in (3) is satisfied. In other words, both the control law $\phi(\cdot)$ and $V(\cdot)$ are typically known functions. Furthermore, from the inequality in (3), it follows that for any $t_\mathrm{i} > t_0$ and $t_\mathrm{f} > t_\mathrm{i}$,

$$\begin{aligned} \Delta V_c &\triangleq V_c(x(t_\mathrm{f})) - V_c(x(t_\mathrm{i})) \\ &= \int_{t_\mathrm{i}}^{t_\mathrm{f}} V_c'(x(t)) f(t, x(t), \phi(x(t)))\mathrm{d}t < 0, \end{aligned} \tag{4}$$

which shows that the Lyapunov function V_c decreases over time along trajectories of (2). We denote by $V_\phi(x(t))$ the value of $V_c(x(t))$ along trajectories of (2).

Now, instead of utilizing a continuous-time control input, we consider a piecewise constant control strategy. Specifically, for the control input vector $u(\cdot) = [u_1(\cdot), \ldots, u_m(\cdot)]^\top$ in (1), let u_σ^*, $\sigma = 1, \ldots, m$, represent a constant value for each corresponding control input $u_\sigma(\cdot)$, $\sigma = 1, \ldots, m$. We define the constant control vector as

$$u^* \triangleq [u_1^*, \ldots, u_m^*]^\top \in \mathbb{R}^m, \tag{5}$$

where $u_\sigma^* > 0$, $\sigma = 1, \ldots, m$. Additionally, we introduce the matrix $M \in \mathbb{R}^{m \times m}$, defined as $M = \mathrm{diag}[\alpha_1, \ldots, \alpha_m]$, where

$$\alpha_\sigma = \begin{cases} 1, & \text{if } u_\sigma \text{ is applied in the positive direction,} \\ -\beta_\sigma, & \text{if } u_\sigma \text{ is applied in the negative direction,} \\ 0, & \text{if } u_\sigma \text{ is not applied,} \end{cases} \tag{6}$$

and $\beta_\sigma > 0$, $\sigma = 1, \ldots, m$, accounts for asymmetric control saturation limits in the positive and negative directions. For simplicity, in the numerical simulations, we assume $\beta_\sigma = 1$, $\sigma = 1, \ldots, m$.

Next, we define the vector

$$u_\mathrm{T} = M u^* = [\alpha_1 u_1^*, \ldots, \alpha_m u_m^*]^\top, \quad t \in [t^*, t^* + \Delta t], \tag{7}$$

as the control input applied to the system in (1) at the time instant t^* for a duration Δt. Now, consider the time interval $t \in [t_\mathrm{i}, t_\mathrm{f}]$, with t_f denoting the time instant when the control input u_T is activated in the system described by (1). The control input over this period is given by

$$u(t) = \begin{cases} 0, & t_\mathrm{i} \leq t < t_\mathrm{f}, \\ u_\mathrm{T}, & t_\mathrm{f} \leq t \leq t_\mathrm{f} + \Delta t, \end{cases} \tag{8}$$

which is the piecewise constant control input applied to the system over the time interval $t \in [t_\mathrm{i}, t_\mathrm{f}]$. We denote by $V_\mathrm{T}(x(t))$ the value of $V_c(x(t))$, where $x(t)$ being the state of the closed-loop system governed by (1) and the control input described by (8).

Thus, over the interval of time $t \in [t_\mathrm{i}, t_\mathrm{f} + \Delta t]$, the value of the Lyapunov function at $t_\mathrm{f} + \Delta t$ is expressed as

$$\begin{aligned} V_\phi \triangleq & V_\phi(x(t_\mathrm{f} + \Delta t)) = V_c(x(t_\mathrm{i})) \\ & + \int_{t_\mathrm{i}}^{t_\mathrm{f} + \Delta t} V_c'(x(t)) f(t, x(t), \phi(x(t)))\mathrm{d}t, \end{aligned} \tag{9}$$

where $x(t)$ is the solution to the closed-loop system (2) with initial conditions $x_0 = x(t_\mathrm{i})$ and $t_0 = t_\mathrm{i}$. Similarly, the value of the Lyapunov function under the control u_T is defined as

$$\begin{aligned} V_\mathrm{T} \triangleq & V_\mathrm{T}(x(t_\mathrm{f} + \Delta t)) = V_c(x(t_\mathrm{i})) \\ & + \int_{t_\mathrm{i}}^{t_\mathrm{f}} V_c'(x(t)) f(t, x(t), 0)\mathrm{d}t + \int_{t_\mathrm{f}}^{t_\mathrm{f} + \Delta t} V_c'(x(t)) f(t, x(t), u_\mathrm{T})\mathrm{d}t, \end{aligned} \tag{10}$$

where in the first integral, $x(t)$ is the solution to (1) with $u(t) \equiv 0$, initial state $x_0 = x(t_\mathrm{i})$ and $t_0 = t_\mathrm{i}$; in the second integral, $x(t)$ is the solution to (1) with $u(t) = u_\mathrm{T}$, initial state $x_0 = x(t_\mathrm{f})$ and $t_0 = t_\mathrm{f}$. When the control duration Δt

Authorized licensed use limited to: City College of New York. Downloaded on January 26,2026 at 02:38:13 UTC from IEEE Xplore. Restrictions apply.

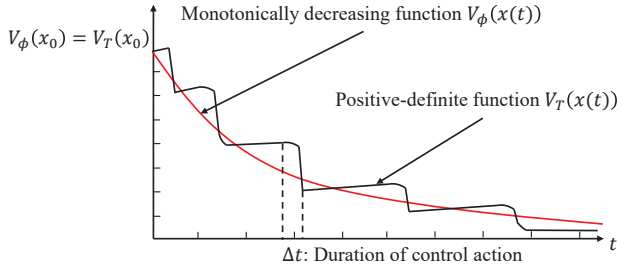

Figure 1: Schematic illustration of functions $V_\phi(x(t))$ and $V_{\mathrm{T}}(x(t))$ over time.

is small, V_{T} can be approximated by

$$V_{\mathrm{T}} \approx V_c(x(t_{\mathrm{i}})) + \int_{t_{\mathrm{i}}}^{t_{\mathrm{f}}} V_c'(x(t)) f(t, x(t), 0)\mathrm{d}t + V_c'(x(t_{\mathrm{f}})) f(t_{\mathrm{f}}, x(t_{\mathrm{f}}), u_{\mathrm{T}})\Delta t. \quad (11)$$

Since $\phi(\cdot)$ is a stabilizing control, inequality (3) guarantees that for any $x \in \mathcal{D}$, there exists a control vector $\phi(x) \in \mathbb{R}^m$ that satisfies (3). Therefore, it is always possible to find $u_{\mathrm{T}} \in \mathbb{R}^m$ such that

$$V_c'(x(t_{\mathrm{f}})) f(t_{\mathrm{f}}, x(t_{\mathrm{f}}), u_{\mathrm{T}}) < 0. \quad (12)$$

One possible approach to selecting u_{T} is to minimize the following expression:

$$u_{\mathrm{T}} = \underset{\alpha_1,\ldots,\alpha_m}{\arg\min} [V'(x(t_{\mathrm{f}})) f(t_{\mathrm{f}}, x(t_{\mathrm{f}}), u_{\mathrm{T}})], \quad (13)$$

subject to (12), where α_σ, $\sigma = 1, \ldots, m$, are defined as in (6).

Given that the value of the Lyapunov function V_ϕ, under the continuous-time control input $\phi(\cdot)$, is guaranteed to converge to zero over time, the control objective is to design the impulsive control inputs u_{T} and their corresponding application times t_{i} in such a way that V_{T} also converges to zero over time. To achieve this objective, we propose the following method and develop a real-time numerical procedure to implement it.

We select the control inputs $u_{\mathrm{T}} \in \mathbb{R}^m$ and their corresponding implementation times $t_{\mathrm{f}} \geq t_0$ such that, after applying the control input to the system described in (1), the following inequality is satisfied

$$\epsilon V_\phi(x(t_{\mathrm{f}}+\Delta t)) < V_{\mathrm{T}}(x(t_{\mathrm{f}}+\Delta t)) < V_\phi(x(t_{\mathrm{f}}+\Delta t)), \quad (14)$$

where $\epsilon \in [0, 1)$ is a design parameter chosen to be close to 1. Consequently, the time evolution of $V_\phi(x(t))$ and $V_{\mathrm{T}}(x(t))$, as illustrated in Figure 1, can be anticipated.

To clarify the numerical procedure associated with our approach, let t_{s} represent the integration sampling time, and define $t_{\mathrm{f}} = t_{\mathrm{i}} + t_{\mathrm{s}}$ as the first instance after t_{i} at which we calculate V_ϕ and V_{T} according to equations (9) and (11), respectively. The control input u_{T} is selected in the form of (7) based on the optimization condition in (13). Given that the integral term in (11) is typically very small due to the narrow integration limits, inequality (14) may not hold, meaning that $V_{\mathrm{T}}(x(t_{\mathrm{f}} + \Delta t))$ could be significantly less than $\epsilon V_\phi(x(t_{\mathrm{f}} + \Delta t))$. In such cases, the control input u_{T} is not applied to the system (1), and the system is allowed to evolve with $u(t) = 0$ until the next sampling time.

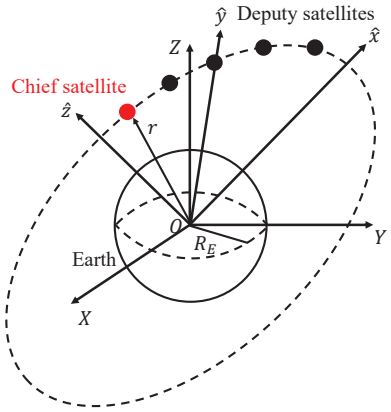

Figure 2: Schematic illustration of SFF system

At the next instance, $t_{\mathrm{f}} = t_{\mathrm{i}} + 2t_{\mathrm{s}}$, the procedure is repeated. If inequality (14) still does not hold, indicating that V_{T} remains significantly smaller than V_ϕ, we again refrain from applying u_{T} and allow the system to continue evolving with $u(t) = 0$ until the next sampling time. This process is repeated until inequality (14) is satisfied. At this moment t_{f}, the control vector u_{T}, obtained from (13), is applied to the system (1). The process then continues by updating the initial time to $t_{\mathrm{i}} = t_{\mathrm{f}} + \Delta t$, and the next control time is set as $t_{\mathrm{f}} = t_{\mathrm{i}} + t_{\mathrm{s}}$, following the same protocol.

It is important to note that at each time step, the numerical algorithm evaluates the values of $V_\phi(x(t_{\mathrm{f}}+\Delta t))$ and $V_{\mathrm{T}}(x(t_{\mathrm{f}}+\Delta t))$ *as if* u_{T} were applied to the system (1) at $t = t_{\mathrm{f}}$. However, the control input u_{T} is actually implemented only at those times t_{f} when inequality (14) is satisfied. Additionally, between these control implementation times, $V_{\mathrm{T}}(x(\cdot))$ may increase. Therefore, the trigger condition in inequality (14) can be supplemented with an additional condition to limit the increase in $V_{\mathrm{T}}(x(\cdot))$ between control applications. This could lead to more frequent control implementations. Lastly, since $\lim_{t\to\infty} V_\phi(x(t)) = 0$, the control strategy ensures that $\lim_{t\to\infty} V_{\mathrm{T}}(x(t)) = 0$, guaranteeing that the closed-loop system state $x(t)$ converges to zero as $t \to \infty$.

3. Coordination Control for Formation Flying of Multiple Satellites

We begin this section by describing the motion equations governing satellite formation flying. Subsequently, utilizing the motion equations we define the error dynamics of the system. Then, two continuous-time feedback control laws are proposed to stabilize the origin of the closed-loop error dynamics. Additionally, we introduce the functions necessary for the mapping of continuous-time control to impulse sequences such as $V_\phi(x(t))$ and $V_{\mathrm{T}}(x(t))$, which are defined in equations (9) and (10) in Section 2, for the satellites formation control.

Authorized licensed use limited to: City College of New York. Downloaded on January 26,2026 at 02:38:13 UTC from IEEE Xplore. Restrictions apply.

System Model

In this section, we introduce the spacecraft formation flying (SFF) system model. Figure 2 presents a schematic of an Earth-orbiting SFF configuration, consisting of a chief satellite and multiple deputy satellites, all in circular orbits. The deputy satellites follow the trajectory of the chief satellite, maintaining a specified distance from the chief and among themselves to preserve the desired formation structure. The inertial coordinate system, denoted as O-XYZ, is fixed at the center of the Earth. In contrast, the perifocal coordinate system O-$\hat{x}\hat{y}\hat{z}$ is also centered at the Earth, with its fundamental plane coinciding with the instantaneous orbital plane. In this system, the unit vector $\hat{x}$ points from the Earth's center towards the instantaneous periapsis, while $\hat{z}$ is normal to the orbital plane and oriented in the direction of the orbital angular momentum vector. The unit vector $\hat{y}$ completes the right-handed coordinate system [16]. Let $q_i = [x_i, y_i, z_i]^\top$ represent the position vector of the i-th satellite in the Earth-Centered Inertial (ECI) reference frame, where $i = 0, 1, 2, 3, \cdots, N$, and subscript 0 to refer to the chief satellite. The equations of motion for the satellite, neglecting the effects of gravitational perturbations and thrust uncertainties, can be written in the ECI frame as follows:

$$\begin{aligned} \ddot{x}_i &= -\frac{\mu}{r_i^3} x_i + u_{i,x}, \\ \ddot{y}_i &= -\frac{\mu}{r_i^3} y_i + u_{i,y}, \\ \ddot{z}_i &= -\frac{\mu}{r_i^3} z_i + u_{i,z}, \end{aligned} \tag{15}$$

where $r_i = ||q_i|| = \sqrt{x_i^2 + y_i^2 + z_i^2}$, μ is the gravitational constant of the Earth, and $u_i = [u_{i,x}, u_{i,y}, u_{i,z}]^\top$ represents the thrust control input.

In this study we assume that the chief satellite follows a predefined circular orbit *without* external interference, meaning the control input for the chief satellite u_0 is zero. Additionally, all deputy satellites are initially positioned and moving along this predefined circular orbit. Furthermore, it is important to note that, unlike centralized control systems where each agent has access to global information and complete situational awareness, in decentralized control each agent can only obtain *local relative* position information with respect to its neighbors. Therefore, in this study, we assume that only the chief satellite knows its global position, while the deputy satellites do not. Each deputy satellite relies solely on local measurements to achieve the global formation task.

Error Dynamics

To establish the error dynamics for the SFF model, we begin by defining the offset vector $l_{i,j}(t) \in \mathbb{R}^3$, $t \geq 0$, which represents the time-varying difference between the generalized position vectors of the i-th and the j-th agents. This vector describes the desired formation of the network, where $i = 1, \cdots, N$, $j \in \mathcal{J}_i$. The set $\mathcal{J}_i$ is defined as:

$$\mathcal{J}_i \subset \{0, 1, \cdots, N\} \setminus \{i\},\ i = 1, \cdots, N,$$

and represents the set of all agents whose position and velocity vectors are available to the i-th agent. In other word, agent $j \in \mathcal{J}_i$ serves as the leader of the agent i. Let the position vectors of the i-th and j-th agents be denoted by $q_i = [x_i, y_i, z_i]^\top$ and $q_j = [x_j, y_j, z_j]^\top$, respectively. The error variable $\tilde{q}_i = [\tilde{q}_{i,x}, \tilde{q}_{i,y}, \tilde{q}_{i,z}]^\top$, which needs to be driven to zero, is defined as:

$$\tilde{q}_i \triangleq q_i - \sum_{j \in \mathcal{J}_i} w_{ij}(q_j + l_{i,j}(t)),\ i = 1, \cdots, N, \tag{16}$$

where $w_{ij} > 0$, $\sum w_{ij} = 1$ represents the weighting factor of each leader agent j relative to follower i. In other words, we assume that the communication network topology among satellites forms a directed spanning tree. It follows that the formation is achieved if the error (16) is driven to zero for each leader-follower pair [17].

Considering the specific satellite formation addressed in this paper, the deputy satellites follow the chief satellite in a sequential manner, with each maintaining a designated distance from its neighboring satellite. We assume that each deputy satellite i has only one leader $i - 1$. Specifically, the chief satellite, denoted by the subscript 0, serves as the leader for the first deputy satellite ($i = 1$), while the first deputy satellite, in turn, acts as the leader for the second deputy satellite ($i = 2$). Consequently, the position and velocity of this leader are measurable for the corresponding deputy. Based on this assumption, the error variable in (16) can be simplified to:

$$\tilde{q}_i \triangleq q_i - q_{i-1} - l_i(t),\ i = 1, \cdots, N, \tag{17}$$

where, with an abuse of notation, $l_i(t) = l_{i,i-1}(t)$. The error dynamics are obtained by taking the second time derivative of (17) and are given by

$$\ddot{\tilde{q}}_i = -\frac{\mu}{r_i^3} q_i + u_i + \frac{\mu}{r_j^3} q_{i-1} - u_{i-1} - \ddot{l}_i(t), \tag{18}$$

where u_i and u_{i-1} denote the control inputs for the i-th and $(i-1)$-th agents, respectively.

It is important to note that, in this study, we assume all satellites are moving within the same circular orbit, and we ignore altitude variations resulting from thruster firings during formation control. Consequently, the magnitude r_i of the position vector q_i is a constant. That is, $r_i = r$ for all $i = 0, 1, \ldots, N$. With this assumption, the error dynamics between the i-th deputy satellite and its leader can be written as

$$\ddot{\tilde{q}}_i = -\frac{\mu}{r^3} (\tilde{q}_i + l_i(t)) - \ddot{l}_i(t) + u_i - u_{i-1}, \tag{19}$$

where $i = 1, \ldots, N$ and $u_0 = 0$, since the chief satellite follows a predefined orbit without any external control input, the term u_0 is zero in this case.

Formation Tracking Control

The objective of decentralized formation control is to design the inputs u_i such that the origin of the error dynamics (19) for all follower agents $i = 1, \cdots, N$ is globally asymptotically stable (GAS).

The procedure for deriving the impulse controller for satellite formation flying begins with designing the continuous control laws u_i to ensure that the origin for (19) is GAS. Subsequently, assuming that the communication topology forms a directed spanning tree we demonstrate that the overall closed-loop multi-agent system exhibits a cascaded structure. By employing the cascade arguments presented in [18], we show that the formation is achieved.

Authorized licensed use limited to: City College of New York. Downloaded on January 26,2026 at 02:38:13 UTC from IEEE Xplore. Restrictions apply.

Formation Control Design I: Backstepping—The stabilization problem for the error system (19) can be solved using the standard backstepping technique. Specifically, define $z_i = \dot{\tilde{q}}_i + k\tilde{q}_i$, where $k > 0$, and consider the following control law

$$u_i = -\frac{\alpha}{\beta}\tilde{q}_i - k\dot{\tilde{q}}_i + \frac{\mu}{r^3}\tilde{q}_i - \lambda z_i + \sum_{j=1}^{i} h_j(t), \tag{20}$$

where $\alpha, \beta, \lambda > 0$, and

$$h_j(t) = \frac{\mu}{r^3} l_j(t) + \ddot{l}_j(t). \tag{21}$$

Note that the function $l_i(t)$ is assigned by the topology designer. Hence, in (20), the term $h_j(t)$ is a time-dependent function that is known in advance of the formation.

Let us first consider the first deputy satellite ($i = 1$) and its leader 0. Under the control law (20) the closed-loop system in error coordinates is then given by

$$\begin{aligned} \dot{\tilde{q}}_1 &= z_1 - k\tilde{q}_1, \\ \dot{z}_1 &= -\frac{\alpha}{\beta}\tilde{q}_1 - \lambda z_1. \end{aligned} \tag{22}$$

The time derivative of the positive definite function

$$V_{c,1} = \frac{1}{2}\alpha\tilde{q}_1^\top\tilde{q}_1 + \frac{1}{2}\beta z_1^\top z_1 \tag{23}$$

is given by

$$\dot{V}_{c,1} = -\alpha k\tilde{q}_1^\top\tilde{q}_1 - \lambda\beta z_1^\top z_1 < 0 \tag{24}$$

for all $\alpha, \beta, \lambda, k > 0$. Therefore, the origin of the closed-loop system (19) is GAS for $i = 1$. For other cases, substituting the controller (20) into the error dynamics (19), the closed-loop error system becomes

$$\begin{aligned} \dot{\tilde{q}}_i &= z_i - k\tilde{q}_i, \\ \dot{z}_i &= -\frac{\alpha}{\beta}\tilde{q}_i - \lambda z_i + \sum_{j=1}^{i-1} h_j(t) - u_{i-1}(t, \tilde{q}_{i-1}, z_{i-1}), \end{aligned} \tag{25}$$

where $i = 2, \ldots, N$. Define $\xi_i = [\tilde{q}_i, z_i]^\top$, and the overall closed-loop multi-agent error dynamics are given by

$$\dot{\xi}_1 = A\xi_1, \tag{26a}$$
$$\dot{\xi}_2 = A\xi_2 + g_1(t, \xi_1), \tag{26b}$$
$$\vdots$$
$$\dot{\xi}_N = A\xi_N + g_{N-1}(t, \xi_{N-1}), \tag{26c}$$

where

$$A \triangleq \begin{bmatrix} -k & 1 \\ -\frac{\alpha}{\beta} & -\lambda \end{bmatrix},$$

$$g_i(t, \xi_i) \triangleq \begin{bmatrix} 0 \\ \sum_{j=1}^{i} h_j(t) - u_i(t, \tilde{q}_i, z_i) \end{bmatrix}.$$

We have the following result.

Theorem 1: Consider the error dynamics (19) and the control law (20) for all $i \in \{1, \cdots, N\}$. Let the control parameters be selected as $\alpha, \beta, \lambda, k > 0$. Then, the formation tracking control problem is solved, and the origin of the closed-loop multi-agent system, $\xi = 0$, where $\xi = [\xi_1^\top, \ldots, \xi_N^\top]^\top$, is GAS. Hence, the desired coordination of the SFF model is achieved.

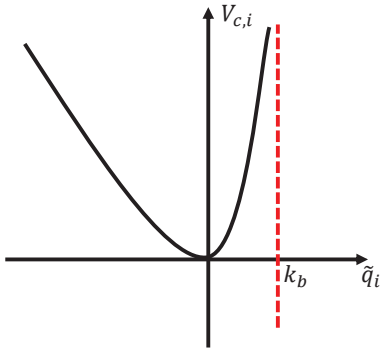

Figure 3: Schematic illustration of Barrier Lyapunov Function

Proof: We complete the proof by induction. First, note that the matrix A is Hurwitz, and thus, for $i = 1$, the origin of (26a) is globally exponentially stable (GES). We have that $\xi_1 = [\tilde{q}_1, z_1]^\top \to 0$ exponentially. For $i = 2$, the system (26a)-(26b) has a cascaded structure. It follows from (20) that

$$g_1(t, \xi_1) = \begin{bmatrix} 0 \\ h_1(t) - u_1(t, \tilde{q}_1, z_1) \end{bmatrix} \to 0 \tag{27}$$

as $\xi_1 \to 0$ because $u_1(t, \tilde{q}_1, z_1) \to h_1(t)$ as $(\tilde{q}_1, z_1) \to 0$. By applying the cascades argument [18, Theorem 2], we conclude that the equilibrium point $(\xi_1, \xi_2) = (0, 0)$ is GES. Denote the system (26a)-(26b) as $\dot{\zeta}_2 = f_{\text{cl},2}(t, \zeta_2)$, where $\zeta_2 \triangleq [\xi_1^\top, \xi_2^\top]^\top$.

Next, for $i = 3$, we have

$$\dot{\zeta}_2 = f_{\text{cl},2}(t, \zeta_2) \tag{28a}$$
$$\dot{\xi}_3 = A\xi_3 + g_2(t, \xi_2), \tag{28b}$$

which is, again, a cascaded system. Note that $g_2(t, \xi_2) \to 0$ as $\zeta_2 \to 0$. Thus, by applying the cascades argument [18, Theorem 2] again, we conclude that the equilibrium point $(\zeta_2, \xi_3) = (0, 0)$ for (28) is GES. Denote the system (28) as $\dot{\zeta}_3 = f_{\text{cl},3}(t, \zeta_3)$, where $\zeta_3 \triangleq [\zeta_2^\top, \xi_3^\top]^\top$. For $i = 4$, the closed-loop system is

$$\dot{\zeta}_3 = f_{\text{cl},3}(t, \zeta_3) \tag{29a}$$
$$\dot{\xi}_4 = A\xi_3 + g_3(t, \xi_3). \tag{29b}$$

The previous arguments, as in the case of $i = 3$, now apply to equations (29). Therefore, the result follows by induction. ■

Formation Control Design II: Backstepping with Barrier Lyapunov Functions—A Barrier Lyapunov Function (BLF) is commonly used in controller design to prevent constraint violations. It ensures that the value of the Lyapunov candidate function becomes infinity as its arguments approach certain predefined limits. For example, Figure 3 provides a schematic illustration of a BLF, where the constraint (or "barrier") is set at k_b. As the system trajectory approaches this limit, the value of the Lyapunov candidate function V grows to

Authorized licensed use limited to: City College of New York. Downloaded on January 26,2026 at 02:38:13 UTC from IEEE Xplore. Restrictions apply.

infinity. This is particularly important for systems subject to constraints such as physical boundaries, saturation limits, or performance and safety specifications [19]. In this study, we introduced a BLF-incorporated backstepping controller for satellite formation flying to mitigate large oscillations in satellite trajectories. The simulation results using this controller are presented in the following section.

Similar to the backstepping approach, we begin by defining the following variable

$$z_i = \dot{\tilde{q}}_i + kP_iR_i\tilde{q}_i + k(I_3 - P_i)\tilde{q}_i \tag{30}$$

where $k > 0$, $I_3 \in \mathbb{R}^{3\times3}$ is the identity matrix, $P_i = \mathrm{diag}(p_{i,x}, p_{i,y}, p_{i,z}) \in \mathbb{R}^{3\times3}$ with

$$\forall\, \eta \in \{x, y, z\},\ p_{i,\eta} = \begin{cases} 0, & \text{if } \tilde{q}_{i0,\eta}(\tilde{q}_{i,\eta} - \tilde{q}_{\mathrm{d}}) > 0, \\ 1, & \text{if } \tilde{q}_{i0,\eta}(\tilde{q}_{i,\eta} - \tilde{q}_{\mathrm{d}}) < 0, \end{cases}$$

where $\tilde{q}_{i0}$ is the initial error of the i-th agent, $\tilde{q}_{\mathrm{d}}$ represents the desired error value. In this paper, since the objective is to achieve a specified formation flying configuration, the desired value $\tilde{q}_{\mathrm{d}}$ is set to zero. Additionally,

$$R_i = \begin{bmatrix} k_b^2 - \tilde{q}_{i,x}^2 & 0 & 0 \\ 0 & k_b^2 - \tilde{q}_{i,y}^2 & 0 \\ 0 & 0 & k_b^2 - \tilde{q}_{i,z}^2 \end{bmatrix},$$

where k_b is the defined limits to which the system trajectory must be constrained. The purpose of setting the values in matrix P_i is as follows: when the system's error state remains on the same side as the initial error state (e.g., if the initial error is negative and the current error is also negative, meaning both lie on the same side of the vertical axis), the corresponding entry in matrix P_i is set to 0. In this case, the control and Lyapunov function behave as in the standard backstepping approach. However, when the error state crosses to the opposite side of the initial state (e.g., if the initial error is negative and the current error becomes positive), the corresponding value in matrix P_i switches to 1, thereby activating the BLF.

Next, applying the control law

$$u_i = \frac{\mu}{r^3}\tilde{q}_i + \sum_{j=1}^{i} h_j(t) - N_i - \frac{\alpha}{\beta}M_i - \lambda z_i, \tag{31}$$

where $\alpha, \beta, \lambda > 0$, $h_j(t)$ is defined in equation (21), and

$$\begin{aligned} M_i &= aP_iR_i^{-1}\tilde{q}_i + (I_3 - P_i)\tilde{q}_i, \\ N_i &= -2kP_iQ_iQ_i\dot{\tilde{q}}_i + kP_iR_i\dot{\tilde{q}}_i + k(I_3 - P_i)\dot{\tilde{q}}_i, \end{aligned}$$

with $a > 0$ and $Q_i = \mathrm{diag}(\tilde{q}_{i,x}, \tilde{q}_{i,y}, \tilde{q}_{i,z})$.

Similarly, consider the pair composed of the first deputy satellite ($i = 1$) and its leader 0, under the control law (31), the closed-loop system in error coordinates becomes

$$\begin{aligned} \dot{\tilde{q}}_1 &= z_1 - kP_1R_1\tilde{q}_1 - k(I_3 - P_1)\tilde{q}_1, \\ \dot{z}_1 &= -\frac{\alpha}{\beta}M_1 - \lambda z_1 \\ &= -\frac{\alpha}{\beta}\left(aP_1R_1^{-1}\tilde{q}_1 + (I_3 - P_1)\tilde{q}_1\right) - \lambda z_1. \end{aligned} \tag{32}$$

Now, we define the Lyapunov function as

$$V_{c,1} = \frac{1}{2}\alpha\left[ap_{1,v}l_{1,v} + \tilde{q}_1(I_3 - P_1)\tilde{q}_1\right] + \frac{1}{2}\beta z_1^\top z_1, \tag{33}$$

where

$$p_{1,v} = [p_{1,x}, p_{1,y}, p_{1,z}], \tag{34a}$$

$$l_{1,v} = \left[\ln\frac{k_b^2}{k_b^2 - \tilde{q}_{1,x}^2}, \ln\frac{k_b^2}{k_b^2 - \tilde{q}_{1,y}^2}, \ln\frac{k_b^2}{k_b^2 - \tilde{q}_{1,z}^2}\right]^\top. \tag{34b}$$

It should be noted that when the value of matrix P_1 is 0, indicating that the BLF is not activated, the Lyapunov candidate function is identical to that of the backstepping approach. Conversely, when the value of matrix P_1 is 1, indicating that the BLF is activated, the logarithmic term in (34b) becomes active. The time derivative of this positive definite function yields

$$\dot{V}_{c,1} = -\alpha ak\tilde{q}_1^\top P_1P_1\tilde{q}_1 - \alpha k\tilde{q}_1^\top(I_3 - P_1)(I_3 - P_1)\tilde{q}_1 - \lambda\beta z_1^\top z_1 < 0, \tag{35}$$

when $a, \alpha, \beta, \lambda, k > 0$. Therefore, the origin of the system (19) is GAS for $i = 1$. For other cases, substituting control law (31) into the error system (19) yields the closed-loop system

$$\begin{aligned} \dot{\tilde{q}}_i &= z_i - kP_iR_i\tilde{q}_i - k(I_3 - P_i)\tilde{q}_i, \\ \dot{z}_i &= -\frac{\alpha}{\beta}M_i - \lambda z_i + \sum_{j=1}^{i-1} h_j(t) - u_{i-1}(t, \tilde{q}_{i-1}, z_{i-1}), \end{aligned} \tag{36}$$

where $i = 2, \cdots, N$. Define $\xi_i = [\tilde{q}_i, z_i]^\top$, and the overall closed-loop multi-agent error dynamics are given by

$$\dot{\xi}_1 = f(\xi_1), \tag{37a}$$

$$\dot{\xi}_2 = f(\xi_2) + g_1(t, \xi_1), \tag{37b}$$

$$\vdots$$

$$\dot{\xi}_N = f(\xi_N) + g_{N-1}(t, \xi_{N-1}), \tag{37c}$$

where

$$f(\xi_i) \triangleq \begin{bmatrix} z_i - kP_iR_i\tilde{q}_i - k(I_3 - P_i)\tilde{q}_i \\ -\frac{\alpha}{\beta}M_i - \lambda z_i \end{bmatrix},$$

$$g_i(t, \xi_i) \triangleq \begin{bmatrix} 0 \\ \sum_{j=1}^{i} h_j(t) - u_i(t, \tilde{q}_i, z_i) \end{bmatrix}.$$

This origin of the closed-loop error dynamics is also GAS. Similar to the procedure used in backstepping controller design I, the proof can be completed by induction. Starting with $i = 1$, note that the origin of the system (37a) is GES according to (35). Therefore, $\xi_1 = [\tilde{q}_1, z_1]^\top \to 0$ exponentially. For $i = 2$, the system (37a)-(37b) forms a cascaded structure. From (31), it follows that $g_1(t, \xi_1) \to 0$ as $\xi_1 \to 0$ because $u_1(t, \tilde{q}_1, z_1) \to h_1(t)$ as $(\tilde{q}_1, z_1) \to 0$. By applying the cascade argument [18, Theorem 2], we conclude that the equilibrium point $(\xi_1, \xi_2) = (0, 0)$ is GES. This induction process can be extended to $i = 3, \ldots, N$, leading to the conclusion that the overall closed-loop system is GAS. Due to space limitations, the detailed proof procedure is omitted in this paper. A comparison of these two different controller approaches for mapping the continuous controller to a discrete controller is presented in the following section.

Authorized licensed use limited to: City College of New York. Downloaded on January 26,2026 at 02:38:13 UTC from IEEE Xplore. Restrictions apply.

Parameters	Symbol	Values	Unit
Standard gravitational parameter	μ	3.9872×10^{14}	m^3/s^2
Earth equatorial radius	R	6378.137	km
Circular orbit altitude	r_a	3622	km
Orbit inclination	ϕ	30	deg
Right ascension of the ascending node	Ω	40	deg
Argument of periapsis	ω	0	deg
Eccentricity	e	0	-
Satellite mass	m	1000	kg

Table 1: Orbital and simulation parameters

Forms of functions V_ϕ and V_{T}—To map the continuous-time controller into an impulse sequence, we define the functions $V_{\phi,i}$ and $V_{\mathrm{T},i}$, whose forms are identical to the Lyapunov function $V_{c,i}$, specifically, for the backstepping controller, these functions are defined as

$$V_{\phi,i} = V_{\mathrm{T},i} = V_{c,i} = \frac{1}{2}\alpha\tilde{q}_i^\top \tilde{q}_i + \frac{1}{2}\beta z_i^\top z_i, \tag{38}$$

and for the BLF-incorporated backstepping controller, they are given by

$$V_{\phi,i} = V_{\mathrm{T},i} = V_{c,i} = \tfrac{1}{2}\alpha\left[a p_{i,v} l_{i,v} + \tilde{q}_i(I_3 - P_i)\tilde{q}_i\right] + \tfrac{1}{2}\beta z_i^\top z_i, \tag{39}$$

where $I_3 \in \mathbb{R}^{3\times 3}$, and

$$p_{i,v} = [p_{i,x}, p_{i,y}, p_{i,z}],$$
$$l_{i,v} = \left[\ln\frac{k_b^2}{k_b^2-\tilde{q}_{i,x}^2}, \ln\frac{k_b^2}{k_b^2-\tilde{q}_{i,y}^2}, \ln\frac{k_b^2}{k_b^2-\tilde{q}_{i,z}^2}\right]^\top.$$

It is important to note that $V_{\phi,i}$, as defined in (9), mirrors the value of $V_{c,i}$ under the continuous-time controller u_i, specifically, (20) for the backstepping controller and (31) for the backsteeping with the BLF. This implies that $V_{\phi,i}$ is a monotonically decreasing function, as shown in (24) and (35), respectively. On the other hand, as expressed in (10), $V_{\mathrm{T},i}$ represents the value of $V_{c,i}$ when using the impulsive controller (8). The value of $V_{\mathrm{T},i}$ is determined by both the impulsive thruster firing time, governed by the condition (14), and the thruster firing duration, which is selected according to (13) for each firing event.

4. NUMERICAL SIMULATION

This section presents the results of simulation studies conducted to demonstrate the effectiveness of the approach for mapping a continuous controller to discrete impulses, as derived in the previous section. In this simulation, a system of five satellites—one chief satellite and four deputy satellites—is considered, forming a circular formation. Throughout the simulation, the chief satellite follows the predefined circular orbit without perturbations or external control input, while the deputy satellites are controlled to track the trajectory of the chief satellite. Initially, all satellites are evenly distributed along the predefined orbit at an altitude of 3622 km, spaced 20 degrees apart. The objective of the formation flying control is to guide the deputy satellites to adjust their positions, rearranging the formation such that each satellite is evenly spaced by 10 degrees relative to the chief satellite by the end of the simulation, which is set to 5400 seconds in this study. The orbital and simulation parameters used in this study are presented in Table 1. In addition to the orbital elements listed in Table 1, the initial phase angles of the satellites are defined as $\theta_0 = [60^\circ, 40^\circ, 20^\circ, 0^\circ, -20^\circ]^\top$. Based on these initial phase angles and the orbital elements, the initial conditions for the positions and velocities of the satellites in the Earth-Centered Inertial (ECI) frame are computed as follows, as described in [16]

$$q_i = \frac{a(1-e^2)}{1+e\cos\gamma_i}\begin{bmatrix}\mathrm{c}_{\gamma_i+\omega}\mathrm{c}_\Omega - \mathrm{c}_\phi\mathrm{s}_{\gamma_i+\omega}\mathrm{s}_\Omega \\ \mathrm{c}_\phi\mathrm{c}_\Omega\mathrm{s}_{\gamma_i+\omega} + \mathrm{c}_{\gamma_i+\omega}\mathrm{s}_\Omega \\ \mathrm{c}_\phi\mathrm{s}_{\gamma_i+\omega}\end{bmatrix}, \tag{41a}$$

$$v_i = \sqrt{\frac{\mu}{a(1-e^2)}}\begin{bmatrix}-\mathrm{c}_\Omega\mathrm{s}_{\gamma_i+\omega} - \mathrm{s}_\Omega\mathrm{c}_\phi\mathrm{c}_{\gamma_i+\omega} - e\big(\mathrm{c}_\Omega\mathrm{s}_\omega + \mathrm{s}_\Omega\mathrm{c}_\omega\mathrm{c}_\phi\big) \\ \mathrm{c}_\Omega\mathrm{c}_\phi\mathrm{c}_{\gamma_i+\omega} - \mathrm{s}_\Omega\mathrm{s}_{\gamma_i+\omega} - e\big(\mathrm{s}_\Omega\mathrm{s}_\omega + \mathrm{c}_\Omega\mathrm{c}_\omega\mathrm{c}_\phi\big) \\ \mathrm{s}_\phi(\mathrm{c}_{\gamma_i+\omega} + e\mathrm{c}_\omega)\end{bmatrix}, \tag{41b}$$

where $\mathrm{c}_x = \cos x$, $\mathrm{s}_x = \sin x$ and $\gamma_i = \theta_i - \omega$ represents the true anomaly of the i-th satellite. Further details are documented in Table 2.

Furthermore, we define the terminal criteria for the multi-agent satellite formation flying control. Specifically, the controller is considered to have successfully achieved its control objectives if the error states $\tilde{q}_i$ and $\dot{\tilde{q}}_i$ meet the following conditions

$$\forall i = 1, \cdots, N,\ ||\tilde{q}_i|| < 0.3\% d_{\mathrm{sep}}$$
$$\forall i = 1, \cdots, N,\ |\dot{\tilde{q}}_{i,x}| < 0.03,\ |\dot{\tilde{q}}_{i,y}| < 0.03\,|\dot{\tilde{q}}_{i,z}| < 0.03, \tag{42}$$

where d_{sep} represents the desired separation distance between the satellites. Specifically, the norm of the position error must be within 0.3% of the desired separation distance, and the absolute values of the velocity errors in all directions must be less than 0.03 km/s at the end of the simulation.

In the following sections, we first present the simulation results of the continuous controller, specifically the backstepping-based controller.

Subsequently, we demonstrate simulation results of satellite formation flying using impulsive control input, in line with the proposed approach for discretizing continuous controllers into an impulsive sequence. In this study, the coefficient ϵ defined in the inequality (14) to adjust the thruster firing instant is set as 0.7. The control forces of the impulsive controller, defined as $f_{\mathrm{T},i} = mu_{\mathrm{T},i}$, remain constant at a magnitude of $f^*_{\mathrm{T},i} = 500$ N throughout the firing duration Δt. The firing duration Δt of the thrusters varies over 19 possible values, ranging from 0.1 seconds to 1 second, in increments of 0.05 seconds. In this section, we introduce and compare the results of mapping two distinct continuous controllers, namely the backstepping controller and the BLF-incorporated backstepping controller, to discrete impulse inputs. This comparison helps to elucidate the motivation for introducing the BLF in the design of the continuous controller. For clarity, this comparison is conducted under a simplified simulation scenario involving one chief satellite and one deputy satellite to focus on the distinctions between the two controllers.

Finally, we present the comprehensive results of satellite formation flying control, applied to four deputy satellites, using discrete impulse inputs.

Results of Continuous-Time Controller

In this section we present the results of applying the continuous controller developed using the backstepping approach for the multi-agent satellite formation flying. The control input is given in equation (20) and the parameters in the controller are defined as $\alpha = 1$,$\beta = 10$, $\lambda = 80$, $k = 0.0001$.

Figure 4 illustrates the Lyapunov functions $V_{c,i}$ for all four deputy satellites over time. As expected from (24), all

Authorized licensed use limited to: City College of New York. Downloaded on January 26,2026 at 02:38:13 UTC from IEEE Xplore. Restrictions apply.

Satellites	$x_0(\times 10^3\,\mathrm{km})$	$y_0(\times 10^3\,\mathrm{km})$	$z_0(\times 10^3\,\mathrm{km})$	$\dot{x}_0(\mathrm{km/s})$	$\dot{y}_0(\mathrm{km/s})$	$\dot{z}_0(\mathrm{km/s})$
Chief	-0.9906	8.9593	4.3301	-5.9466	-1.4205	1.5786
Deputy 1	2.2900	9.1884	3.2139	-5.8019	0.6000	2.4186
Deputy 2	5.2945	8.3092	1.7101	-4.9574	2.5482	2.9668
Deputy 3	7.6604	6.4279	0	-3.5150	4.1891	3.1572
Deputy 4	9.1024	3.7712	-1.7101	-1.6487	5.3246	2.9668

Table 2: Initial conditions of satellites

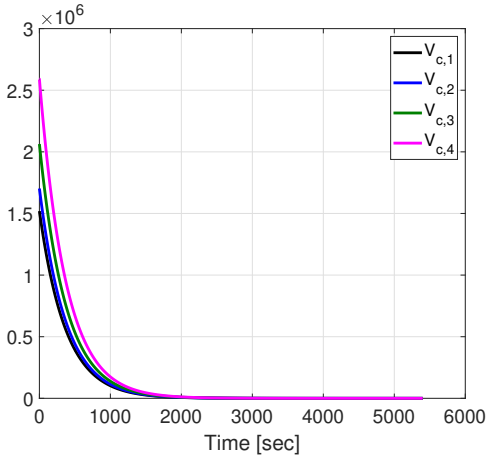

Figure 4: Plots of Lyapunov function $V_{c,i}$ using backstepping continuous controller versus time

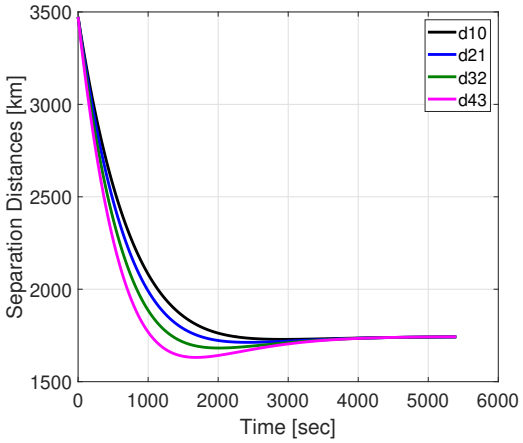

Figure 5: Separation distances of satellites using backstepping continuous controller.

plots exhibit monotonic decrease in the Lyapunov functions, reflecting the stability of the system. Figure 5 depicts the separation distances between two adjacent satellites, specifically, the plot labeled $d10$ represents the distance between the chief satellite and the first deputy satellite, while the plot $d21$ shows the distance between the first and second deputy satellites. Notably, as shown in Figure 5, the initial separation distances of approximately 3500 km converge to 1743 km. This distance corresponds to the expected separation for satellites that are 10 degrees apart at this altitude, indicating that the continuous controller successfully achieves the control objective.

The continuous-time control inputs for the first deputy satellite, shown in Figure 6, reveal a significant initial magnitude, which corresponds to the large initial errors in the system states at the start of the simulation. It is worth noting that the observed thrust magnitudes exceeding 10×10^4 N may not be feasible in practical scenarios. This highlights the necessity of the proposed approach, which inherently accounts for control saturation limits within the design.

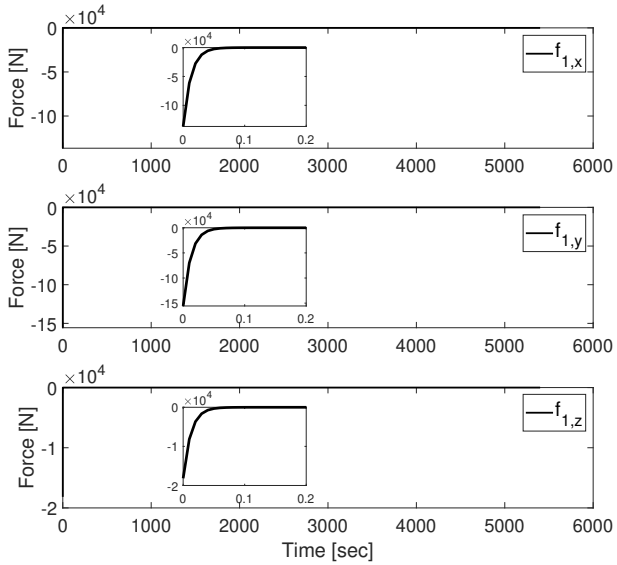

Figure 6: Control input of the first deputy satellite using backstepping continuous controller.

Results of Discrete Impulse Controller: 1 Chief and 1 Deputy Satellite

In this section, we present the results of using the impulse controller for the formation control scenario involving one chief satellite and one deputy satellite. Specifically, we transform the continuous controllers, which are developed based on the backstepping approach and the BLF-incorporated backstepping approach, into a discrete firing sequence. This transformation is performed according to the mapping approach proposed in Section 2, utilizing the functions $V_{\phi,i}$ and $V_{\mathrm{T},i}$ as defined in (38) and (39) for the backstepping controller and the BLF-incorporated backstepping controller, respectively.

Results of the Impulsive Controller Discretized from Backstepping Controller—The forms of functions $V_{\phi,i}$ and $V_{\mathrm{T},i}$ for backstepping controller are given in (38). Parameters for the functions used to mapping the continuous controller to impulsive input are set as $\alpha = 1$, $\beta = 10$, $\lambda = 80$, and $k = 0.0001$.

Figure 7 presents the plots of functions $V_{\phi,1}$ and $V_{\mathrm{T},1}$. Note that function $V_{\phi,1}$ is identical to Lyapunov function $V_{c,1}$

Authorized licensed use limited to: City College of New York. Downloaded on January 26,2026 at 02:38:13 UTC from IEEE Xplore. Restrictions apply.

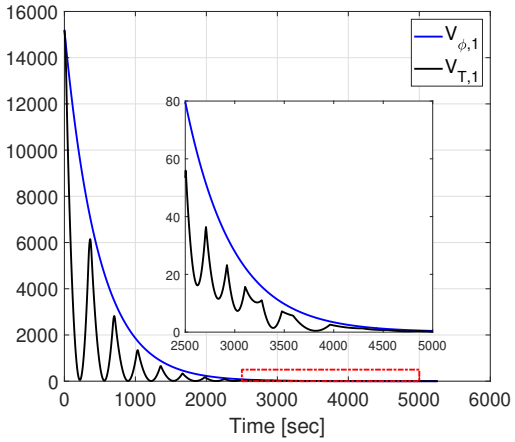

Figure 7: Plots of $V_{\phi,1}$ and $V_{\mathrm{T},1}$ using discretized impulsive controller based on backstepping controller versus time.

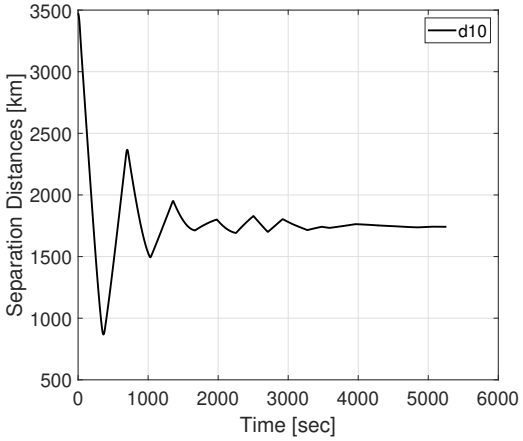

Figure 8: Separation distances between the chief and first deputy satellites using impulsive controller discretized from backstepping controller.

and, as expected, exhibits a monotonic decrease over time. Additionally, while the values of $V_{\mathrm{T},1}$ may increase between the instants of impulsive control implementation, the overall trend of $V_{\mathrm{T},1}$ remains decreasing, closely following the behavior of $V_{\phi,1}$ over time.

Figures 8 and 9 present the separation distances between the chief and deputy satellite, as well as the error states, $\tilde{q}_1$ and $\dot{\tilde{q}}_1$ of the deputy satellite, respectively. While the impulsive controller successfully achieves the control objective—namely, converging the separation distances between the satellites to the desired value and ensuring all error states fall within the terminal criteria—significant oscillations are observed in the results. For example, the error state $\tilde{q}_{1,x}$ exhibits oscillations with a maximum amplitude exceeding 1000 km. These oscillations arise because, despite the proximity of the error states to the desired values (i.e., approaching zero), the function $V_{\phi,1}$ consistently remains below $V_{\mathrm{T},1}$, thereby delaying thruster activation required for effective deceleration. A key drawback of such pronounced oscillations is the increased energy consumption due to the repeated adjustments necessary to counteract these oscillations. This can be observed in Figure 10, which presents the firing sequence of the impulsive controller discretized from the backstepping controller. To mitigate the oscillations and thereby achieve energy savings, we propose an approach based on discretizing the BLF-incorporated backstepping controller, with the corresponding results presented in the next section.

Results of the Impulsive Controller Discretized from BLF-incorporated Backstepping Controller—This section presents the simulation results of the impulsive controller discretized based on the BLF-incorporated backstepping controller. The functions $V_{\phi,i}$ and $V_{\mathrm{T},i}$ used for discretizing the BLF-incorporated controller are defined in (39). Parameters in the equations (39) used for discretizing the continuous controller into an impulse sequence are defined as $\alpha = 1$, $\beta = 10$, $\lambda = 80$, $k = 0.0001$, and $a = 10^5$.

It is important to emphasize that the value of $V_{\mathrm{T,i}}$ should not be confused with $V_{\phi,i}$. Although these functions share the same form, $V_{\phi,i}$ reflects the value of the Lyapunov function $V_{c,i}$, which is derived based on the closed-loop system's states under the continuous controller. As a result, $V_{\phi,i}$ is monotonically decreasing. In contrast, the value of $V_{\mathrm{T},i}$ depends on the impulsive controller's firing instants and durations.

As introduced in Section 3, when the error trajectory exceeds zero from the side of the initial error state, the corresponding value in matrix P_i switches to 1, thereby activating the logarithmic term in (39). As the trajectory approaches the predefined limit k_b (set to 100 in this study), the value of the function $V_{\mathrm{T,i}}$ increases sharply and tends toward infinity.

We leverage this property of the BLF in our discretization approach: when a component $\tilde{q}_{i,\eta}$ (where $\eta \in \{x, y, z\}$) of the error vector $\tilde{q}_i$ exceeds zero from the side of the initial error state and approaches the limit, the value of $V_{\mathrm{T,i}}$ increases rapidly, even if the absolute error remains small. Since the logarithmic term is activated, $V_{\mathrm{T,i}}$ rises above $V_{\phi,i}$, prompting control actions to reduce the corresponding error state $\dot{\tilde{q}}_{i,\eta}$, thereby mitigating overshoot in $\tilde{q}_{i,\eta}$ and ultimately alleviating oscillations. The value of a is set sufficiently large, at 10^5 in this study, to ensure that the value of the function $V_{\mathrm{T,i}}$ rises sharply above $V_{\phi,i}$ once the logarithmic term is activated.

Therefore, in addition to the thruster selection criterion given by (13), when a value in matrix P_i equals 1 and $V_{\mathrm{T,i}}$ exceeds $V_{\phi,i}$, we enforce that the discrete control input $u_{\mathrm{T,i}}$ is selected according to

$$u_{\mathrm{T},i} = \underset{\alpha_1,\ldots,\alpha_m}{\arg\min} |\dot{\tilde{q}}_{i,\eta}(t_{\mathrm{f}} + \Delta t)|, \tag{43}$$

subject to (12), where $i = 1, \cdots, N$.

Figure 11 shows the trajectories of the functions $V_{\phi,1}$ and $V_{\mathrm{T},1}$ using impulsive thruster mapping from the BLF-incorporated backstepping controller over the simulation period. The plot for $V_{\phi,1}$ exhibits a monotonically decreasing behavior, which is consistent with expectations. The operational principle of the BLF is evident in the trajectory of $V_{\mathrm{T},1}$. As the value of an error state crosses zero, the logarithmic term in (39) is activated, leading to a sharp increase in the value of $V_{\mathrm{T},1}$. The red-circled spikes on the plot of $V_{\mathrm{T},g}$ in Figure 11 highlight these sudden increases.

Figures 12 and 13 depict the separation distance between the chief and deputy satellite, along with the error state trajectories $\tilde{q}_1$ and $\dot{\tilde{q}}_1$ over time, using the discretized input

Authorized licensed use limited to: City College of New York. Downloaded on January 26,2026 at 02:38:13 UTC from IEEE Xplore. Restrictions apply.

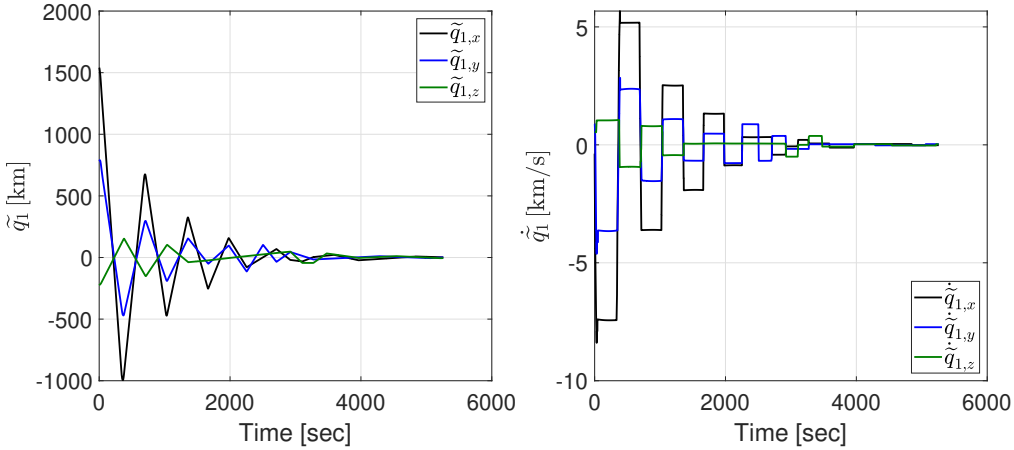

Figure 9: Error states $\tilde{q}_1$ and $\dot{\tilde{q}}_1$ of the deputy satellite using discretized impulsive controller based on backstepping controller over time.

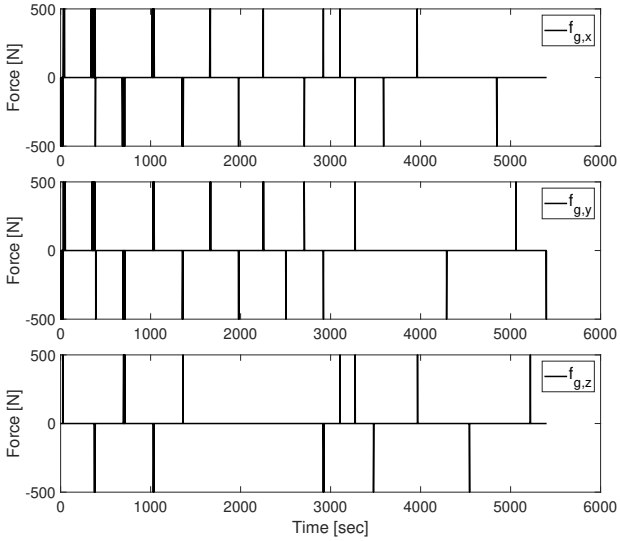

Figure 10: Firing sequence of impulsive controller discretized from the backstepping controller.

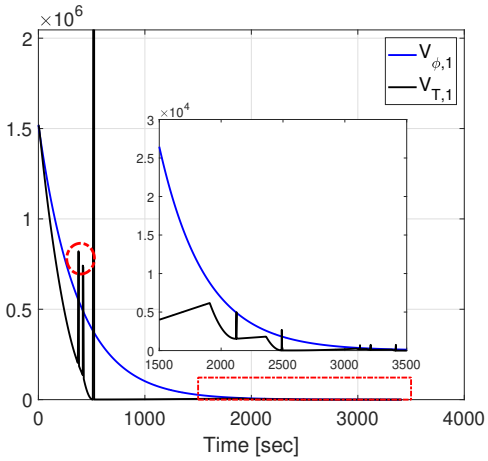

Figure 11: Plots of $V_{\phi,1}$ and $V_{\mathrm{T},1}$ using discretized impulsive controller based on BLF-incorporated backstepping controller versus time.

transformed from the BLF-incorporated backstepping controller. It is evident that the issue of significant oscillations, observed in Figures 8 and Figure 9, has been effectively resolved. All error states converge to stability and meet the terminal criteria defined in (42), and the separation distance between the two satellites also converges to the desired value efficiently.

The firing sequences of the impulsive controller, discretized from the BLF-incorporated backstepping controller, are illustrated in Figure 14. It is evident that at each firing event, the thrusters fire at a constant magnitude of 500 N. The difference between each firing lies in the duration, which is determined by either (13) or (43), depending on the value of matrix P_i. Compared to the impulsive firing sequence discretized from the conventional backstepping controller shown in Figure 10, the discrete input mapping from the BLF-incorporated backstepping controller demonstrates improved energy efficiency.

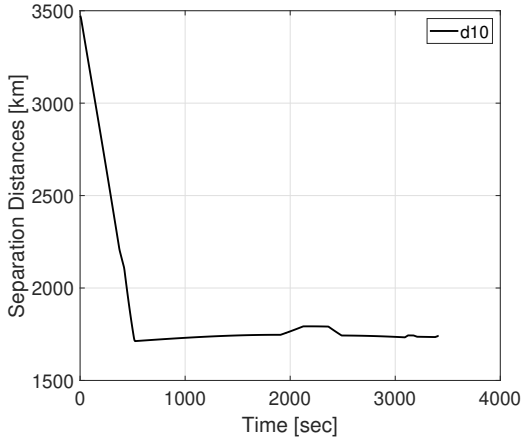

Figure 12: Separation distances between the chief and first deputy satellites using impulsive controller discretized from BLF-incorporated backstepping controller.

Authorized licensed use limited to: City College of New York. Downloaded on January 26,2026 at 02:38:13 UTC from IEEE Xplore. Restrictions apply.

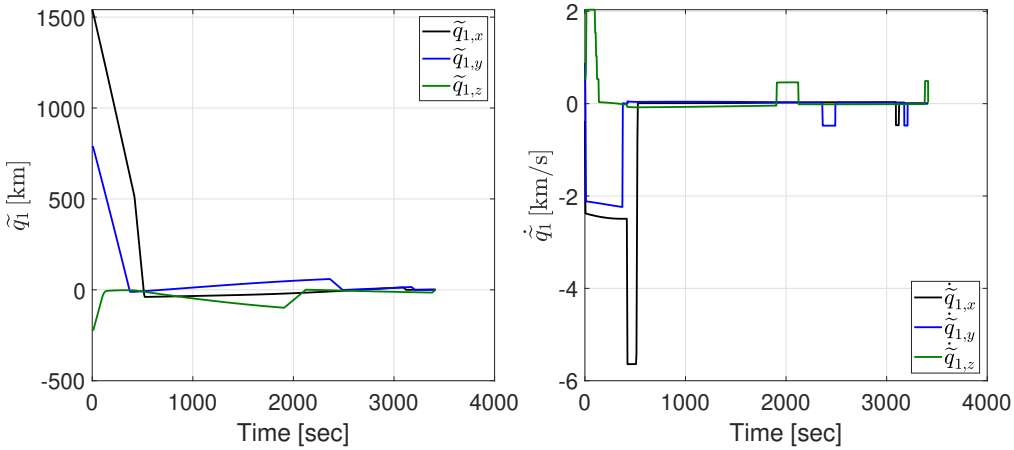

Figure 13: Error states $\tilde{q}_1$ and $\dot{\tilde{q}}_1$ of the deputy satellite using discretized impulsive controller based on BLF-incorporated backstepping controller over time.

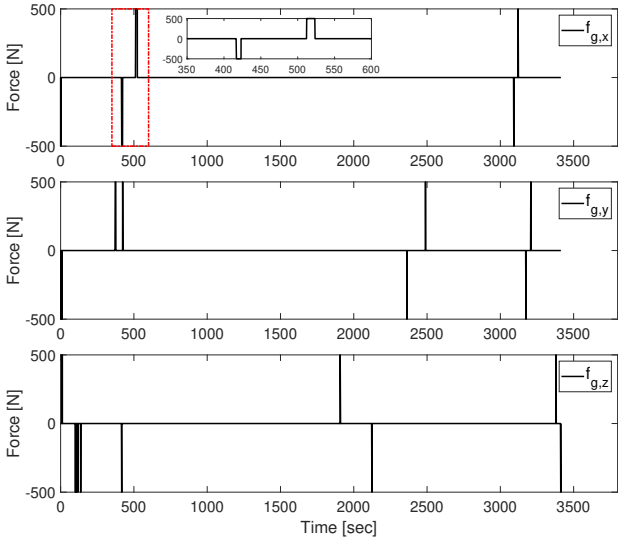

Figure 14: Firing sequence of impulsive controller discretized from the BLF-incorporated backstepping controller.

Results of Discrete Impulse Controller: 1 Chief and Multiple Satellites

In this section, we present the results of decentralized multi-satellite formation control using the impulsive inputs discretized from the continuous BLF-incorporated backstepping controller. Parameters setting for functions $V_{\phi,i}$ and $V_{\mathrm{T},i}$ used for discretizing the continuous controller into an impulse sequence are defined as $\alpha = 1$, $\beta = 10$, $\lambda = 80$, $k = 0.0001$, and $a = 10^5$.

The simulation scenario is consistent with the previous setup, where five satellites are initially positioned in a predefined circular orbit, spaced 20 degrees apart from one another. The chief satellite follows the prescribed orbit without perturbation or control input, while the four deputy satellites are guided to track the chief satellite's trajectory using only local information. The goal of the formation control is to adjust the deputy satellites' positions, reconfiguring the formation so that each satellite is evenly spaced by 10 degrees relative to the chief satellite. The initial conditions of all satellites are provided in Table 2.

Figures 15 and 16 depict the trajectories of all satellites and the separation distances between adjacent satellites, respectively. Starting from different initial conditions, it is evident that under the control of the discretized impulsive controller, the positions of all deputy satellites are successfully rearranged, with all satellites converging to the desired separation distance. Figures 17 and 18 illustrate the error states $\tilde{q}_i$ and $\dot{\tilde{q}}_i$ for all deputy satellites. Although larger oscillations are observed in the error states $\tilde{q}_3$ and $\tilde{q}_4$—corresponding to the two deputy satellites at the rear of the formation—all error states ultimately converge to sufficiently small values, ensuring compliance with the termination criteria proposed in (42). These larger oscillations can be attributed to the decentralized control strategy, where errors propagate along the formation, accumulating from the leading agents to the trailing ones, thereby resulting in relatively more significant oscillations in $\tilde{q}_3$ and $\tilde{q}_4$. Despite this, the overall system achieves the desired objective.

In addition, the energy consumption for each deputy satellite using the continuous-time controller and the discrete impulsive controller is calculated as follows

$$E_{\phi,i} = \int_{t_0}^{t_{\mathrm{end}}} u_i^\top u_i \, dt \tag{44}$$

and

$$E_{\mathrm{T},i} = u_{\mathrm{T},ix}^2 \Delta t_{i,x} + u_{\mathrm{T},ix}^2 \Delta t_{i,y} + u_{\mathrm{T},ix}^2 \Delta t_{i,z}, \tag{45}$$

where t_0 and t_{end} represents the simulation start and end times, u_i is the continuous-time control input, and $u_{\mathrm{T},i} = [u_{\mathrm{T},ix}, u_{\mathrm{T},iy}, u_{\mathrm{T},iz}]^{\mathrm{T}}$ denotes the discrete impulsive control input. Furthermore, the energy saving percentage is given by

$$\text{Energy Saving } \% = \frac{E_{\phi,i} - E_{\mathrm{T},i}}{E_{\phi,i}} \times 100. \tag{46}$$

The results are summarised in Table 3. It is evident that as the position of the satellites progresses toward the tail of the formation, energy consumption increases. This can be attributed to two factors. First, to achieve the desired satellite formation, the error state $\tilde{q}_i$ that needs to be eliminated becomes larger

Authorized licensed use limited to: City College of New York. Downloaded on January 26,2026 at 02:38:13 UTC from IEEE Xplore. Restrictions apply.

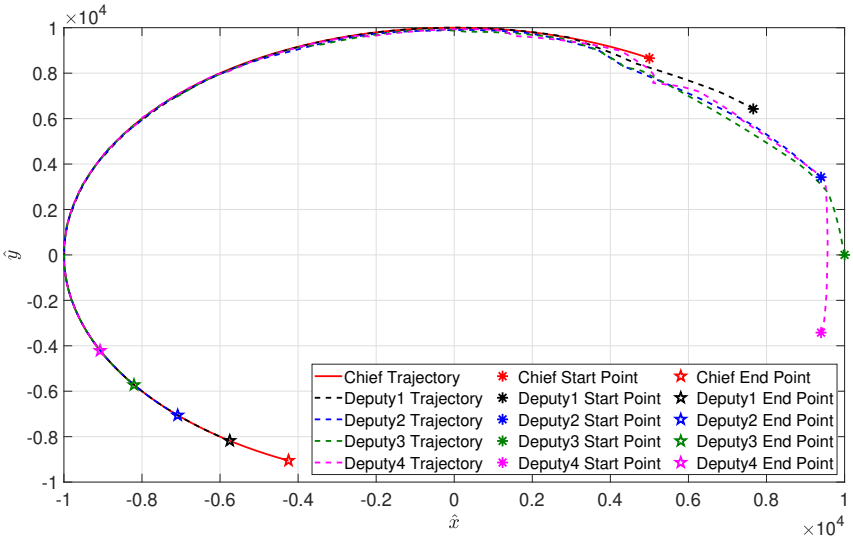

Figure 15: Satellite trajectories shown in orbit plane using impulsive control discretized from BLF-incorporated backstepping controller.

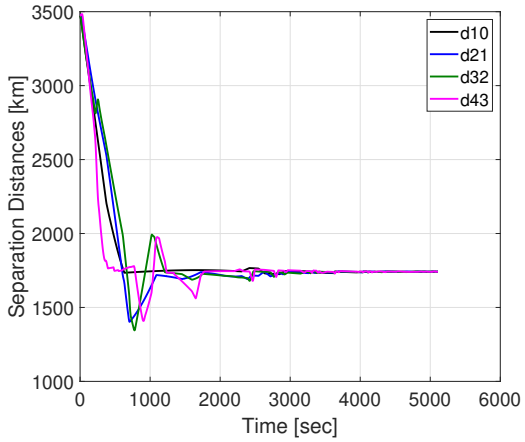

Figure 16: Separation distances of adjacent satellites in the five-satellite formation using impulsive controller discretized from BLF-incorporated backstepping controller.

as the satellite's position moves further back in the queue. Second, errors in decentralized control tend to propagate and accumulate toward the tail of the formation, further increasing energy consumption. Moreover, when comparing the energy consumption of each deputy satellite, the discrete controller demonstrates significant energy savings, reducing energy consumption by more than 90% compared to the continuous-time controller.

5. Conclusion

In this paper, we presented a novel technique utilizing Lyapunov arguments to convert an existing continuous-time control input into a sequence of discrete impulses while ensuring the desired performance of the closed-loop system. The core concept of our approach is a real-time numerical algorithm that identifies the timing of control impulse injections by comparing the value of a Lyapunov function under continuous-time control with that under impulsive control. The primary objective of this control strategy is to maintain the value of the Lyapunov function under impulsive control below that of continuous-time control. As the latter approaches zero over time, the impulsive control ensures a reduction in the Lyapunov function's value to zero, thereby achieving the desired performance. We applied this framework to the decentralized control of satellite formation flying and evaluated two different continuous controllers while discretizing the continuous controller into impulsive inputs. Simulation results demonstrated that the discretized controller effectively achieves the control objectives and shows potential for energy savings compared to the continuous-time controller. In addition, the proposed technique includes the control saturation limits as the inherent part of the design.

References

[1] H. K. Khalil, *Nonlinear Systems*, 3rd ed. Upper Saddle River, NJ: Prentice-Hall, 2002.

[2] W. M. Haddad and V. Chellaboina, *Nonlinear Dynamical Systems and Control. A Lyapunov-Based Approach*. Princeton, NJ: Princeton University Press, 2008.

[3] R. Yanushevsky, *Modern Missile Guidance*. Boca Raton, FL: CRC Press, 2007.

[4] H. Ashrafiuon, "Guidance and attitude control of unstable rigid bodies with single-use thrusters," *IEEE Trans. Control Sys. Tech.*, vol. 25, no. 2, pp. 401–413, 2017.

[5] J. Ragazzini and G. Franklin, *Sampled-Data Control Systems*. New York, NY: McGraw Hill, 1958.

[6] T. Chen and B. Francis, *Optimal Sampled-Data Control Systems*. London: Springer, 1995.

[7] D. Jeong and W. Jeon, "Performance of adaptive sleep period control for wireless communications systems," *IEEE Trans. Wireless Commun.*, vol. 5, no. 11, pp. 3012–3016, 2006.

[8] H. Kong, G. C. Goodwin, and M. M. Seron, "A cost-effective sparse communication strategy for networked

Authorized licensed use limited to: City College of New York. Downloaded on January 26,2026 at 02:38:13 UTC from IEEE Xplore. Restrictions apply.

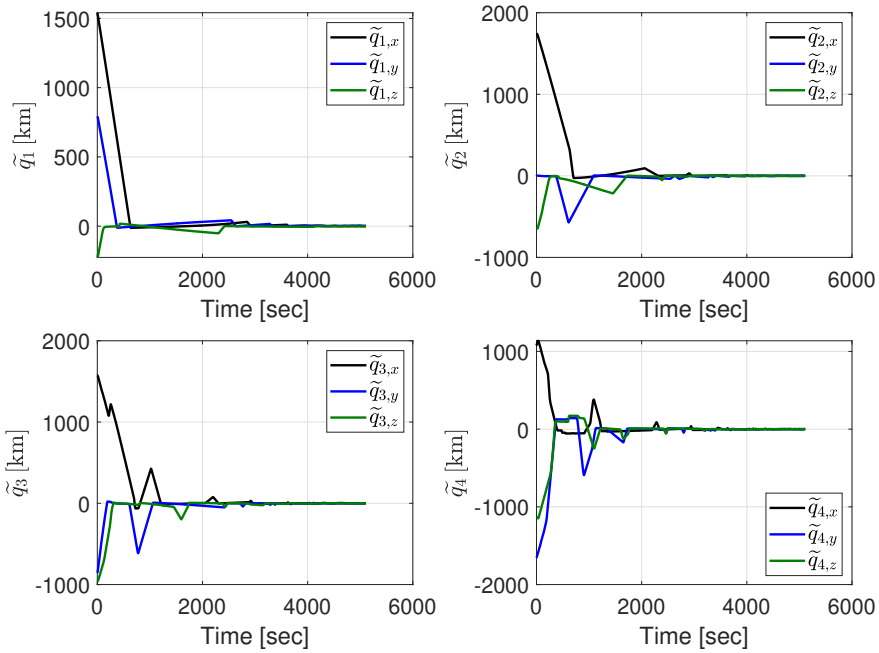

Figure 17: Error states $\tilde{q}_1$ of all deputy satellites using impulsive controller discretized from BLF-incorporated backstepping controller.

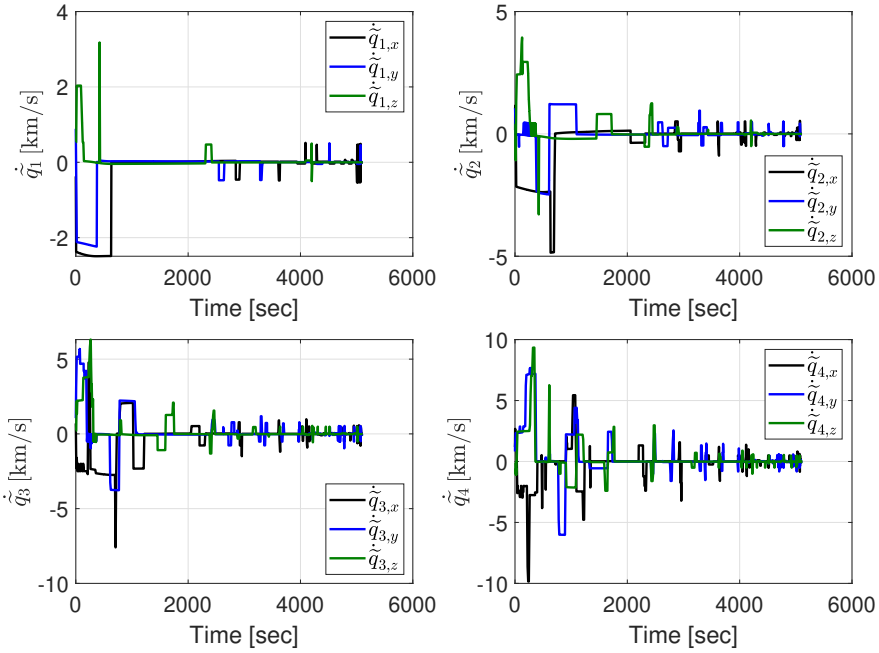

Figure 18: Error states $\dot{\tilde{q}}_1$ of all deputy satellites using impulsive controller discretized from BLF-incorporated backstepping controller.

Satellites	Discrete controller	Continuous controller	Energy Saving %
Deputy 1	24.7750	324.9642	92.37
Deputy 2	59.4250	699.8369	91.51
Deputy 3	84.8750	1205.0579	92.96
Deputy 4	114.8425	2128.9211	94.61

Table 3: Comparison of energy consumption for all deputy satellites using continuous and discrete controllers.

Authorized licensed use limited to: City College of New York. Downloaded on January 26,2026 at 02:38:13 UTC from IEEE Xplore. Restrictions apply.

linear control systems: An svd-based approach," *Int. J. Robust Nonlin. Contr.*, vol. 25, no. 4, pp. 2223–2240, 2014.

[9] M. Nagahara, D. Quevedo, and J. Østergaard, "Sparse packetized predictive control for networked control over erasure channels," *IEEE Trans. Autom. Contr.*, vol. 59, no. 7, pp. 1899–1905, 2014.

[10] M. Nagahara, D. Quevedo, and D. Nešić, "Maximum hands-off control: A paradigm of control effort minimization," *IEEE Trans. Autom. Contr.*, vol. 61, no. 3, pp. 735–747, 2016.

[11] S. Schaanning, B. Kristiansen, and J. Gravdahl, "Maximum hands-off attitude control," in *Proc. Amer. Contr. Conf.*, Atlanta, GA, 2022, pp. 4003–4010.

[12] R. W. Brockett, "Minimum attention control," in *Proc. IEEE Conf. Dec. Contr.*, San Diego, CA, 1997, pp. 2628–2632.

[13] M. Donkers, P. Tabuada, and W. Heemels, "Minimum attention control for linear systems," *Discrete Event Dynam. Syst.*, vol. 24, no. 2, pp. 199–218, 2014.

[14] M. Donkers and W. Heemels, "Output-based event-triggered control with guaranteed $\mathcal{L}_\infty$-gain and improved and decentralised event-triggering," *IEEE Trans. Autom. Contr.*, vol. 57, pp. 1362–1376, 2012.

[15] A. Anta and P. Tabuada, "To sample or not to sample: self-triggered control for nonlinear systems," *IEEE Trans. Autom. Contr.*, vol. 55, pp. 2030–2042, 2010.

[16] K. T. Alfriend, S. R. Vadali, P. Gurfil, J. P. How, and L. S. Breger, *Chapter 2 - Fundamental Astrodynamics*, K. T. Alfriend, S. R. Vadali, P. Gurfil, J. P. How, and L. S. Breger, Eds. Oxford: Butterworth-Heinemann, 2010.

[17] B. Wang, S. G. Nersesov, and H. Ashrafiuon, "Time-varying formation control for heterogeneous planar underactuated multivehicle systems," *Journal of Dynamic Systems, Measurement, and Control*, vol. 144, no. 4, p. 041006, 2022.

[18] E. Panteley and A. Loria, "On global uniform asymptotic stability of nonlinear time-varying systems in cascade," *Systems & Control Letters*, vol. 33, no. 2, pp. 131–138, 1998.

[19] K. Tee, S. Gea, and E. Tay, "Barrier Lyapunov functions for the control of output-constrained nonlinear systems," *Automatica*, vol. 45, pp. 918–927, 2009.

Authorized licensed use limited to: City College of New York. Downloaded on January 26,2026 at 02:38:13 UTC from IEEE Xplore. Restrictions apply.